Asian Journal of Chemistry; Vol. 36, No. 9 (2024), 2160-2168

ASIAN JOURNAL OF CHEMISTRY

https://doi.org/10.14233/ajchem.2024.32199

Enhanced Structural, Optical and Magnetic Properties of Cobalt-Doped Zinc Oxide Nanoparticles Synthesized *via* Co-Precipitation Method

PRAVEENA PANNEER SELVAM[1], VADAMALAR RATHINAM[1,*], AMEER BAIG ALI BAIG[2] and R. SAGAYARAJ[3,*]

[1]Department of Physics, Muthurangam Government Arts College (Affiliated to Thiruvalluvar University, Tamilnadu), Vellore-632002, India
[2]Department of Physics, St. Joseph College of Arts and Science for Women (Affiliated to Periyar University), Salem-636304, India
[3]PG & Research Department of Physics, St. Joseph's College of Arts and Science (Autonomous) (Affiliated to Annamalai University, Tamilnadu), Cuddalore-607001, India

*Corresponding authors: E-mail: vadamalarvnb@yahoo.co.in; sagayarajnancy@gmail.com

Received: 5 June 2024; *Accepted*: 10 August 2024; *Published online*: 30 August 2024; AJC-21743

This study reported the synthesis and characterization of cobalt-doped zinc oxide (Co-ZnO) nanoparticles using the co-precipitation method with a focus on their structural, optical and magnetic properties. Pure ZnO and Co-ZnO nanoparticles were synthesized and compared to evaluate the effects of cobalt doping. X-ray diffraction (XRD) analysis revealed that cobalt doping led to a reduction in peak intensities and an increase in lattice strain, indicating successful substitution of Co^{2+} ions into the ZnO lattice. The average particle size of Co-ZnO nanoparticles decreased from 9.41 nm to 3.82 nm, with a corresponding increase in specific surface area from 1.17×10^{14} m^2/g for pure ZnO to 1.65×10^{14} m^2/g for Co-ZnO. UV-visible spectroscopy showed a blue shift in the absorption edge for Co-ZnO nanoparticles, with an energy band gap of 3.36 eV compared to 3.25 eV for pure ZnO exhibiting enhanced UV absorption capabilities. Photoluminescence (PL) spectra highlighted the presence of violet-blue and blue-green emissions, suggesting improved photocatalytic properties due to Co doping. Transmission electron microscopy (TEM) and energy-dispersive X-ray spectroscopy (EDX) confirmed the hexagonal shape and successful incorporation of cobalt ion into the ZnO lattice. Vibrating-sample magnetometry (VSM) measurements revealed a significant increase in magnetization for Co-ZnO nanoparticles demonstrating enhanced ferromagnetic properties with a magnetic moment of 0.5198 T. This study concludes that cobalt doping significantly enhances the structural, optical, magnetic and photocatalytic properties of ZnO nanoparticles, making them suitable for applications in photocatalysis, gas sensing and spintronics.

Keywords: ZnO nanoparticles, Cobalt, Co-precipitation method, UV-Vis spectroscopy, Photoluminescence, Magnetic properties.

INTRODUCTION

Zinc oxide nanoparticles with their diverse applications ranging from metal products to ceramics, ointments and the medical field, exemplify the potential of nanotechnology in various sectors [1-3]. Zinc oxide exhibits two main crystalline structures *viz*. cubic zinc blende and hexagonal wurtzite. Under ambient conditions, the wurtzite structure is thermodynamically more stable than zinc blende. ZnO is a II-VI semiconductor with a direct band gap of approximately 3.37 eV and a binding energy of 60 meV. These properties make it a highly attractive candidate for the synthesis of sustainable nanoparticles. Doping ZnO with transition metal oxides (TMOs) such as Co, Mn, Fe, Ni and Cr can significantly alter its physical, chemical, optoelectronic and magnetic properties. This has led to remarkable advancements in the development of solar cells, sensors, piezoelectric devices and spintronic devices [4-7].

This study investigates the incorporation of cobalt ions into the ZnO crystal lattice. The larger ionic radius of Zn^{2+} (0.74 Å) compared to Co^{2+} (0.70 Å) allows for potential substitution within the structure. Fabricating magnetic semiconducting materials presents a significant challenge for researchers developing spintronic devices. These devices require efficient manipulation of spin-polarized carriers, including injection, transport and control. Achieving the room-temperature ferromagnetism in nanoparticles has proven particularly difficult. Several methods are available to synthesize the doped materials such as wet precipitation method [8,9], sol-gel method [10,11], chemical co-precipitation method [12], combustion method [13], *etc*.

As cobalt doping in zinc oxide nanostructures increases band gap energy with increasing dopant concentration [14], therefore, it is possible to fabricate various-sized nanorods [15]. Chanda *et al.* [16] explored the magnetic properties of cobalt-doped ZnO nanoparticles. Their findings, based on field dependent magnetization measurements, suggest the coexistence of diamagnetic, superparamagnetic and ferromagnetic behaviours at room temperature. Meky *et al.* [17] observed that enhancement in the lattice strain with Co doping could be attributed to the size and ionic radius difference between Zn and Co ions. Cobalt-doped ZnO exhibits enhanced photocatalytic activity due to its ability to minimize electron-hole pair recombination and its porous structure [18]. Previous studies have reported that Co-ZnO nanoparticles exhibit high dielectric properties and a decreasing band gap trend, suggesting their potential for low-frequency devices such as optoelectronics, photodetectors and spintronics [19]. Co-ZnO nanoparticles have also shown to exhibit superior gas sensing properties for methane compared to pure ZnO nanoparticles [20,21]. Additionally, Co-doped ZnO thin films possess excellent non-linear optical properties, making them promising for optical devices and non-linear power control applications [22]. With their reduced particle size and increased surface-to-volume ratio, the unexpected impacts of specific surface area (SSA) on nanoparticles are apparent [23]. This study aims to investigate the influence of cobalt doping on the structural, morphological, optical, magnetic and luminescent properties of ZnO nanoparticles synthesized by the co-precipitation method. The findings of this study contributed to the development of ZnO-based nanomaterials with tailored properties for applications including photocatalysis, gas sensing, spintronics and optoelectronics.

EXPERIMENTAL

All the chemicals used in this study were of analytical grade (AR) with 99.99% purity. Zinc nitrate hexahydrate, cobalt nitrate hexahydrate and sodium hydroxide served as the precursors for Zn, Co and OH, respectively.

Synthesis: Cobalt-doped zinc oxide nanoparticles (Co-ZnO) were prepared in a 3:1 ratio using the co-precipitation method. A 0.75 M solution of $Zn(NO_3)_2{\cdot}6H_2O$ in 50 mL of deionized water was stirred at 60 ºC for 6 h. Simultaneously, a 0.25 M solution of $Co(NO_3)_2{\cdot}6H_2O$ in 50 mL of deionized water was stirred under the same conditions. Both solutions were mixed and 0.6 g of cetyltrimethylammonium bromide (CTAB) was added to prevent agglomeration followed by the addition of ammonia solution dropwise to adjust the pH to 13, resulting in the formation of pale pink precipitate. The suspension was stirred for an additional 2 h. The obtained colloidal precipitate was filtered, washed repeatedly with ethanol and dried in a silica crucible at 120 ºC for 3 h. Subsequent annealing at 400 ºC for 2 h in a muffle furnace yielded yellowish-white Co-ZnO nanoparticles. Pure ZnO nanoparticles were synthesized using the same procedure, substituting zinc nitrate and sodium hydroxide as precursors.

RESULTS AND DISCUSSION

Structural analysis: The XRD patterns of pure ZnO and Co-ZnO are shown in Fig. 1. X-ray diffraction was carried out with a wavelength of $\lambda = 0.15406$ nm. The miller indices (*hkl*) values of the synthesized pure ZnO nanoparticles were (002), (101), (102), (110), (103), (112), (201), (004) and (202) at the position of 2θ (34.23º, 36.05º, 47.40º, 56.37º, 62.69º, 67.69º, 68.71º, 72.38º and 76.84º) for ZnO (JCPDS card no. 89-0510) [24]. For Co-ZnO NPs, the values are (101), (110), (103) and (201) at the position of 2θ (31.62º, 36.40º, 56.51º, 63.02º, (JCPDS card No. 00-001-1149) [25]. The broadened X-ray diffraction peaks indicate that the crystalline has a small size with a polycrystalline nature. It could be observed that the peak intensity of Co-ZnO NPs are lesser when compared to pure ZnO spectrum. It may be due to the size of ionic radius of Zn^{2+} (0.74 Å), which is greater than ionic radius of Co^{2+} (0.58 Å). Hence after substitution of Co^{2+} in to the Zn^{2+} lattice, resulting an appreciable decrease in its diffraction peak intensities [26]. From Fig. 1, a sharp peak at 36.28 nm confirms the substitution of cobalt ions into the ZnO lattice. Table-1 gives the average crystalline size of the nanoparticles at different 2θ values with their respective FWHW values for both ZnO and Co-ZnO NPs. Tables 2 and 3 shows various peaks of both ZnO

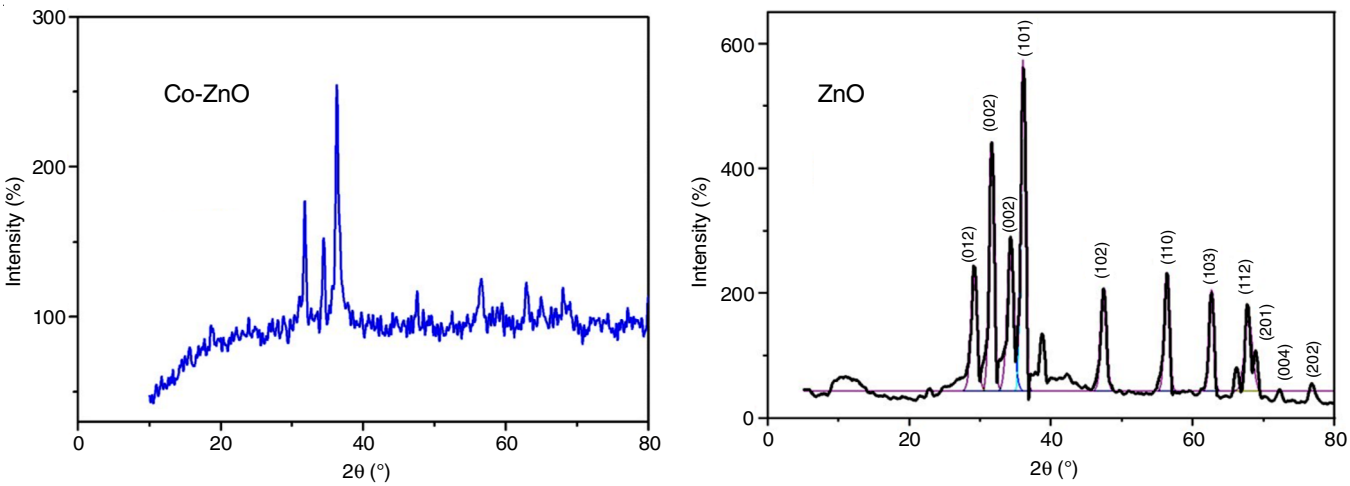

Fig. 1. X-ray diffraction (XRD) patterns of pure ZnO and Co-doped ZnO nanoparticles

TABLE-1
STRUCTURAL PARAMETERS OF SYNTHESIZED Co-ZnO NANOPARTICLES

	Lattice parameters	Angle	Structure	Size (nm)
ZnO	a = 3.2530 Å; c = 5.20730 Å	α = β = 90°; γ = 120°	Hexagonal	9.41
Co-ZnO	a = b = c = 9.72 Å	α = β = γ = 90°	Cubic	3.38

TABLE-2
PARTICLE SIZE (D), SPECIFIC SURFACE AREA (SSA), MORPHOLOGY INDEX (M.I.), DISLOCATION DENSITY (δ) AND MICROSTRAIN (ε) OF ZnO

Position, 2θ (°)	FWHM β (rad)	D (nm)	SSA × 10^{-14} (m^2 g^{-1})	M.I.	δ (10^{-16} m^2)	ε
29.10	0.5079	7.77	1.37	0.699	1.66	0.489
31.59	0.5513	10.00	1.06	0.682	1.00	0.487
34.24	0.5977	7.11	1.50	0.664	1.98	0.485
36.05	0.6292	10.76	0.99	0.653	0.86	0.483
47.38	0.8260	9.29	1.15	0.588	1.16	0.471
56.32	0.9831	10.87	0.98	0.546	0.85	0.459
62.63	1.0930	12.17	0.87	0.520	0.67	0.449
67.84	1.1841	7.31	1.46	0.500	1.87	0.440
Average		9.41	1.17	0.606	1.25	0.471

TABLE-3
PARTICLE SIZE (D), SPECIFIC SURFACE AREA (SSA), MORPHOLOGY INDEX (M.I.), DISLOCATION DENSITY (δ) AND MICROSTRAIN (ε) OF Co-ZnO NANOPARTICLES

Position, 2θ (°)	FWHM β (rad)	D (nm)	SSA × 10^{-14} (m^2 g^{-1})	M.I.	δ (10^{-16} m^2)	ε
11.53	0.0408	3.41	1.21	0.990	8.60	0.101
30.91	0.0867	1.66	2.49	0.978	36.34	0.078
36.35	0.0157	9.27	0.45	0.996	1.16	0.012
57.86	0.1113	1.42	2.90	0.972	49.40	0.050
64.63	0.0488	3.36	1.23	0.987	8.85	0.019
Average		3.28	1.65	0.829	20.87	0.052

and Co-ZnO NPs size, specific surface area, morphology index, dislocation density and microstrain. The average particle size of synthesized doped nanoparticles has been estimated using the Debye-Schererr's formula [26]. The interplanar spacing between atoms (d-spacing) was calculated using Bragg's law whereas the particle size was calculated from the following expressions:

$$2d \sin\theta = n\lambda$$

$$D = \frac{0.9\lambda}{\beta\cos\theta}$$

where D is the crystallite diameter size; λ is the wavelength of X-ray (0.15406 nm); β is the full-width half maximum intensity of peak (FWHM) and θ is diffracted angle incident X-ray on the sample. The specific surface area (SSA) was computed using the following formula [27]:

$$SSA = \frac{6000}{D\times\rho}$$

where ρ is the density of doped nanoparticles and D is the particle size.

Tables 2 and 3 show the average specific surface area of the synthesized ZnO and Co-ZnO nanoparticles to be 1.17 × 10^{14} m^2/g and 1.65 × 10^{14} m^2/g, respectively. A larger specific surface area indicates more exposed surface sites, which can enhance reactivity and adsorption properties. ZnO nanoparticles with such a small specific surface area might be suitable for applications like UV light absorbers, photocatalysis and gas sensors. The increase in specific surface area due to cobalt doping suggests enhanced surface reactivity. The dislocation density (δ) is the length of dislocation lines per unit volume of the crystal and the larger dislocation density implies a larger hardness. The formula used to determine dislocation density (δ) [27] as

$$\delta = \frac{1}{D^2}$$

where δ is dislocation density and D is crystallite size of the samples, the average dislocation density (δ) of sample to be using the above expression is also given in Tables 2 and 3. The ZnO nanoparticles with an average specific surface area of approximately 1.17 × 10^{14} m^2/g exhibit unique characteristics, whereas the Co-doped ZnO nanoparticles with an average specific surface area of approximately 1.65 × 10^{14} m^2/g offers enhanced properties. The morphological index (M.I.) were calculated obtained by using below equation:

$$M.I. = \frac{FWHM_h}{(FWHM_h + FWHM_p)}$$

where $FWHM_h$ is the highest full-width half-maximum (FWHM) intensity value among the peaks, while $FWHM_p$ is the FWHM of particular peak for which M.I. was calculated. A higher M.I. value in Co-doped ZnO indicates improved crystallinity.

Micro strain is the degree of distortion of lattice planes that gives rise to non-uniform changes in the interplanar spacings present in the crystalline lattice [28] and was calculated using the following equation:

$$\varepsilon = \frac{\beta}{4\tan\theta}$$

here β is FWHM (full-width half maximum intensity of peak), θ is the diffracted angle incident X-ray on the sample. Tables 2 and 3 show that the average particle size of Co-ZnO decreases from 9.41 nm to 5.60 nm due to the substitution of Co^{2+} for Zn^{2+} in the lattice. This reduction is likely caused by the lattice surface disorder and induced strain in ZnO (0.471) and Co-ZnO (0.052). Doping with Co^{2+} ions hinders the growth of ZnO grains, resulting in the decreased diffraction peak intensity due to the internal lattice stress [29].

UV spectral studies: Absorption spectra of both samples were measured in the wavelength range of 200 nm to 800 nm to investigate the effect of cobalt doping on ZnO absorption, as depicted in Fig. 2. The cut-off wavelength for pure ZnO and Co-ZnO nanoparticles was determined to be 345 nm and 385 nm, respectively. The observed spectrum reveals a small dip in the absorption peak from 312 nm to 354 nm. Due to the size distribution of Co-ZnO nanoparticles, smaller particles exhibit a blue shift in their absorption edge due to the quantum confinement [30,31] indicated that smaller particles absorb at shorter wavelengths. The interaction between excitons (electron-hole pairs) and phonons (lattice vibrations) can influence the absorption spectrum, leading to dips or shoulders in the peak. The introduction of cobalt into the ZnO lattice can modify the electronic structure, potentially introducing new energy levels or altering existing ones and thus affecting the absorption spectrum. Defects in the crystal structure, such as oxygen vacancies or zinc interstitials, can create localized energy states within the bandgap, leading to absorption bands [32]. Particle aggregation can lead to interference effects in the absorption spectrum, resulting in dips or shoulders. The UV emission band originates from the radiative recombination of excitons on the surfaces of ZnO nanoparticles, while the visible emission band is attributed to transitions associated with deep levels caused by the

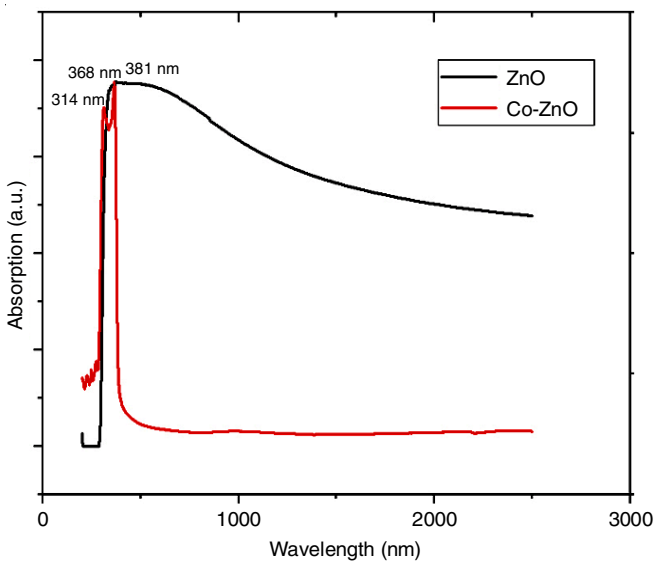

Fig. 2. UV-visible absorption spectra of ZnO and Co-ZnO nanoparticles

oxygen vacancies [33]. The optical property of Co-ZnO depends strongly on the synthesis conditions and type of material used.

The energy band gap structure of Co-ZnO was determined from the UV-Vis absorption spectra using the following relations [34]:

$$I = I_o e^{-\alpha t}$$

$$E = h\nu = \frac{hc}{\lambda}$$

$$(\alpha h\nu)^n = A(h\nu - E_g)$$

where I is the intensity of transmitted light; I_o is the intensity of incident light; t is the sample thickness; α is the absorption coefficient; h is Planck's constant; c is the speed of light; λ is the wavelength, A is a constant and n = 2 represents a direct band and n = ½ represents an indirect band gap.

Fig. 3 represents the Tauc plots of the direct band gap for both synthesized ZnO and Co-ZnO nanoparticles [35]. For Co-ZnO NPs, the cut-off wavelength is 385 nm, indicating that it absorbs light in the ultraviolet region, while for ZnO, the cut-off wavelength is at 345 nm. A larger band gap corres-

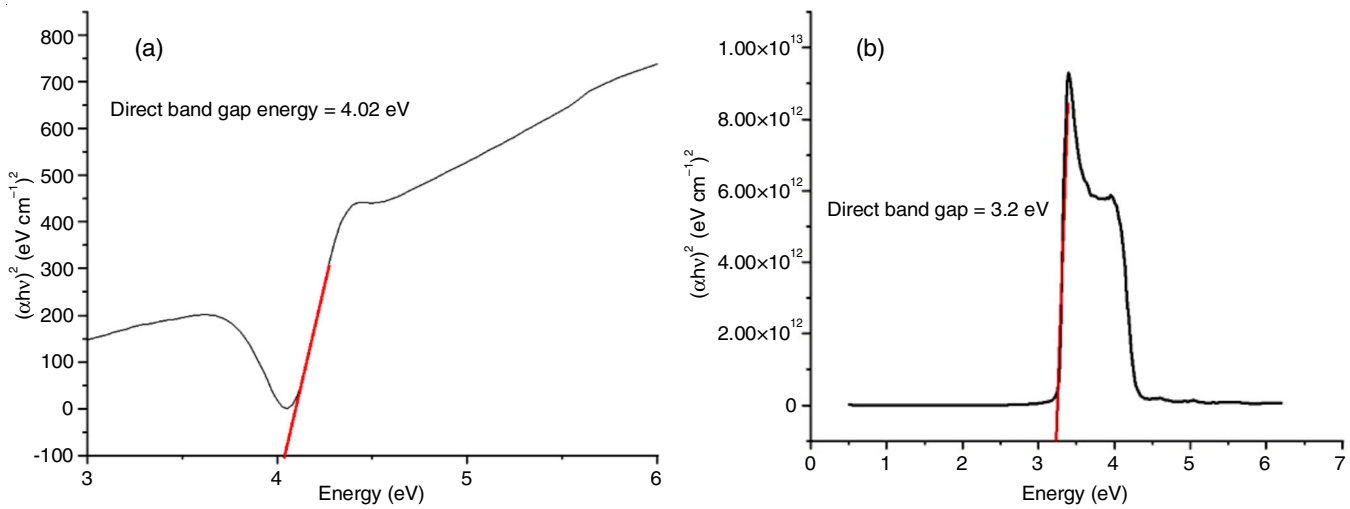

Fig. 3. Tauc plots for ZnO (a) and Co-ZnO (b) nanoparticles

ponds to a wider range of non-absorption (transparent) wavelengths. Co-ZnO has a direct energy band gap of 3.2 eV, while ZnO has a slightly smaller band gap of 4.02 eV and observed in Table-4. Co-ZnO smaller band gap suggests it can absorb higher energy photons (shorter wavelengths), making it suitable for UV applications.

TABLE-4
DATA'S ON UV-VISIBLE SPECTROSCOPY

Optical absorption	Co-ZnO	ZnO
Cut-off wavelength	368 nm	381 nm
Energy band gap (E_g)	3.36 eV	3.254 eV

Photoluminescence (PL) studies: The PL spectra of Co-ZnO nanoparticles in the 350-600 nm range are shown in Fig. 4. The PL spectra exhibit violet-blue and blue-green emission peaks at 423 nm and 486 nm, respectively as well as a UV-NBE emission peak at approximately 371 nm. The emission peak at 423 nm suggests the presence of zinc vacancies, as the energy gap between the zinc vacancy level and the conduction band is nearly 3.0 eV. The emission peak at 486 nm indicates an electron transition from the ionized oxygen vacancy level to the valence band. The emission peak at about 371 nm, located near the 380 nm region reported in [36] is likely attributed to band-to-band exciton transition [37]. The peak at ~ 371 nm primarily originates from band-edge emission due to the radiative annihilation of excitons, which can also be attributed to the recombination of free and shallowly bound electrons [38]. Additionally, the peak at 486 nm may be associated with the formation of hydroxyl radicals and surface defects. Although the PL spectra of ZnO and Co-ZnO are quite similar, the increased intensity in the case of Co-ZnO nanoparticles could be due to the nanoparticles acting as quenching centers for donor-acceptor pairs involving Co ions within the ZnO crystal structure [29]. This suggests that Co-ZnO nanoparticles may effectively contribute to the photocatalytic degradation of organic pollutants.

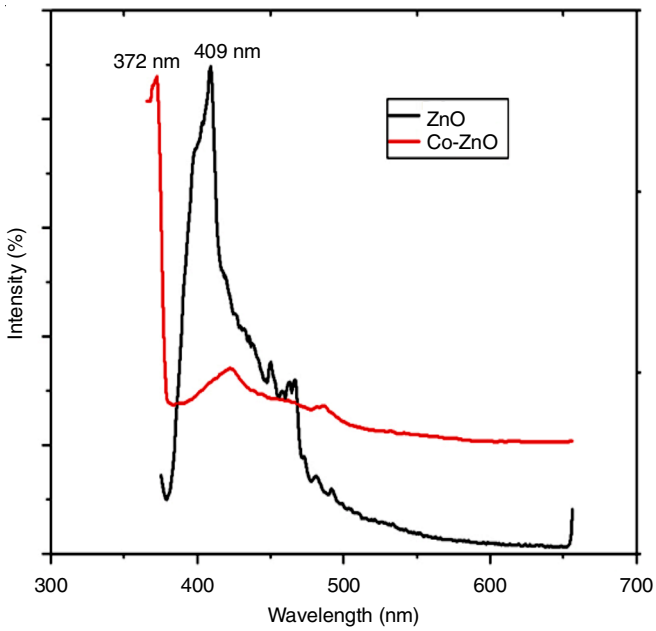

Fig. 4. Photoluminescence (PL) spectra of ZnO and Co-ZnO

Morphological studies: Morphological studies and energy dispersive X-ray analysis (EDAX) of both ZnO and Co-ZnO nanoparticles are shown in Figs. 5 and 6, which clearly shows that both ZnO and Co-ZnO nanoparticles exhibit a hexagonal shape and are closely packed. This study reported a significant morphological change from spherical to rod-like nanoparticles following Co doping as observed through TEM micrographs. Compared to ZnO nanoparticles, Co doped ZnO nanoparticles exhibited a more significant tendency for agglomeration because of interparticle interactions. Specifically, Co-ZnO nanoparticles formed aggregates in the size range of 10 to 50 nm.

Fig. 7a compares the EDAX spectra of Co-ZnO and ZnO NPs, while Fig. 7b provides a magnified view of the Co-ZnO spectrum. The Co-ZnO nanoparticles exhibited more distinct concentric circles in the SAED pattern compared to ZnO nanoparticles [39]. According to the spectra, both samples contained Zn, O, Co elements only and no other elements found in either sample confirming the purity of both materials.

FTIR spectral studies: The FTIR spectrum of pure ZnO typically exhibits characteristic peaks attributed to Zn-O stretching and bending vibrations as shown in Fig. 8. Peaks at 434, 454, 513 and 593 cm^{-1} are associated with Zn-O stretching vibrations [40], whereas at 870 and 1029 cm^{-1} could be assigned to Zn-O bending modes or potentially surface-related vibrations [41]. Peaks at 1386 and 1452 cm^{-1} might indicate the presence of carbonate species, possibly adsorbed from the atmosphere during sample preparation [41,42]. A peak at 1644 cm^{-1} is often associated with the bending vibration of adsorbed water molecules [43]. The characteristic C-H stretching vibrations observed at 2855 and 2914 cm^{-1} suggest the presence of organic contaminants or incomplete precursor removal [44]. A strong peak at 3469 cm^{-1} is typically attributed to the O-H stretching vibration of adsorbed water.

The introduction of cobalt into the ZnO lattice can influence its vibrational properties [45]. The additional peaks in the Co-doped ZnO spectrum compared to pure ZnO provide insights into cobalt incorporation and potential structural modifications. New peaks at 774, 933, 1017, 1098, 1180, 1210, 1245, 1338 and 1438 cm^{-1} are likely due to the formation of Co-O bonds or interactions between cobalt and the ZnO lattice [46]. They might also indicate alterations in the Zn-O vibrational modes caused by the presence of cobalt. Similar to pure ZnO, peaks at 1612 and 1693 cm^{-1} might be related to adsorbed water or carbonate species [47]. Peaks in the higher frequency region (1797, 1874, 1916, 1989, 2044 and 2121 cm^{-1}) are less common in metal oxide spectra [48]. They could be attributed to overtones or combination bands of existing vibrations, or they might originate from impurities or residual precursors.

VSM studies: VSM data offers insights into the magnetic properties of ZnO and Co-ZnO samplesas shown in Fig. 9. The zinc oxide nanoparticles exhibits a low magnetization (M_s) of 8.9046×10^{-6} emu indicating weak ferromagnetic behaviour [49,50]. The high coercivity (H_c) value of 391.88 Oe suggests significant resistance to magnetization reversal [51], whereas the low retentivity (M_r) value of 258.53×10^{-6} emu reflected in low remnant ratio (R) of 0.029, which implies the minimal residual magnetization after removing the external field [52].

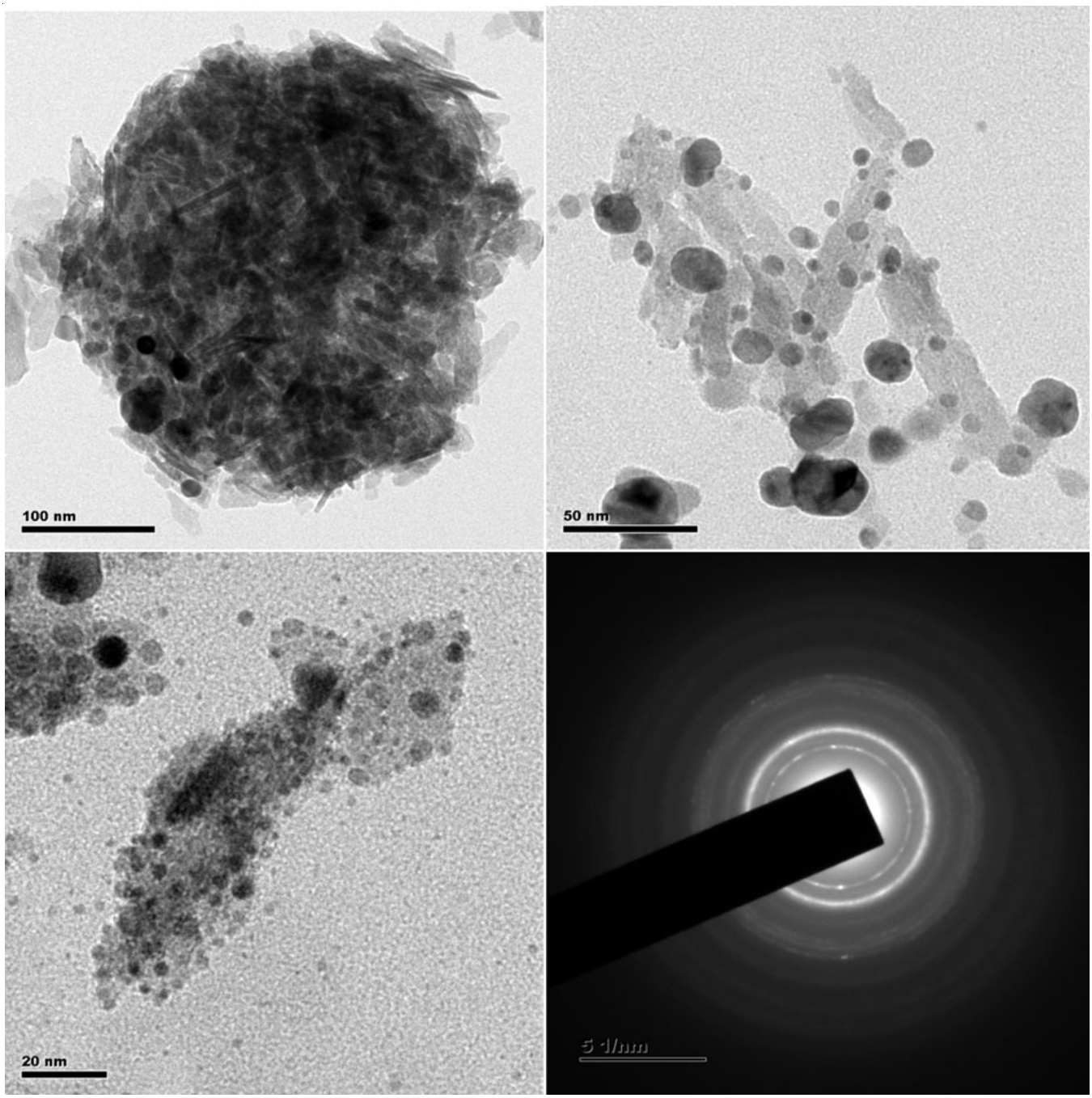

Fig. 5. Transmission electron microscopy (TEM) images of ZnO nanoparticles at different magnifications

The magnetic moment (μ_B) of 0.00012975 Tesla is negligible, whereas the anisotropy constant (K) of 3.6349 erg g^{-1} suggests a low energy barrier for magnetization reversal (Table-5).

Overall, ZnO nanoparticles demonstrate feeble magnetic properties [52,53], in contrast, Co-ZnO nanoparticles shows a substantially higher magnetization (M_s) of 11448×10^{-3} emu, indicative of enhanced ferromagnetic characteristics. The coercivity (H_c) of 315.13 Oe is lower than ZnO suggesting easier magnetization reversal. The retentivity (M_r) of 213.11×10^{-6} emu and remnant ratio (R) of 0.000018 are also lower, implying less residual magnetization. However, the magnetic moment (μ_B) of 0.5198 Tesla is significantly higher signifying a consi-

TABLE-5
DATA'S ON MAGNETIZATION (Ms), COERCIVITY (Hci), RETENTIVITY (Mr), MAGNETIC MOMENT (μ_B), REMNANT RATIO (R) AND ANISOTROPY CONSTANT (K)

Sample	Ms (emu)	Hci (Oe)	Mr (emu)	μ_B (Tesla)	R = Mr/Ms	K (erg/g)
ZnO	8.9046×10^{-3}	391.88	258.53×10^{-6}	0.00012975	0.029000	3.6349
Co-ZnO	11448×10^{-3}	315.13	213.11×10^{-6}	0.51980000	0.000018	3757.92

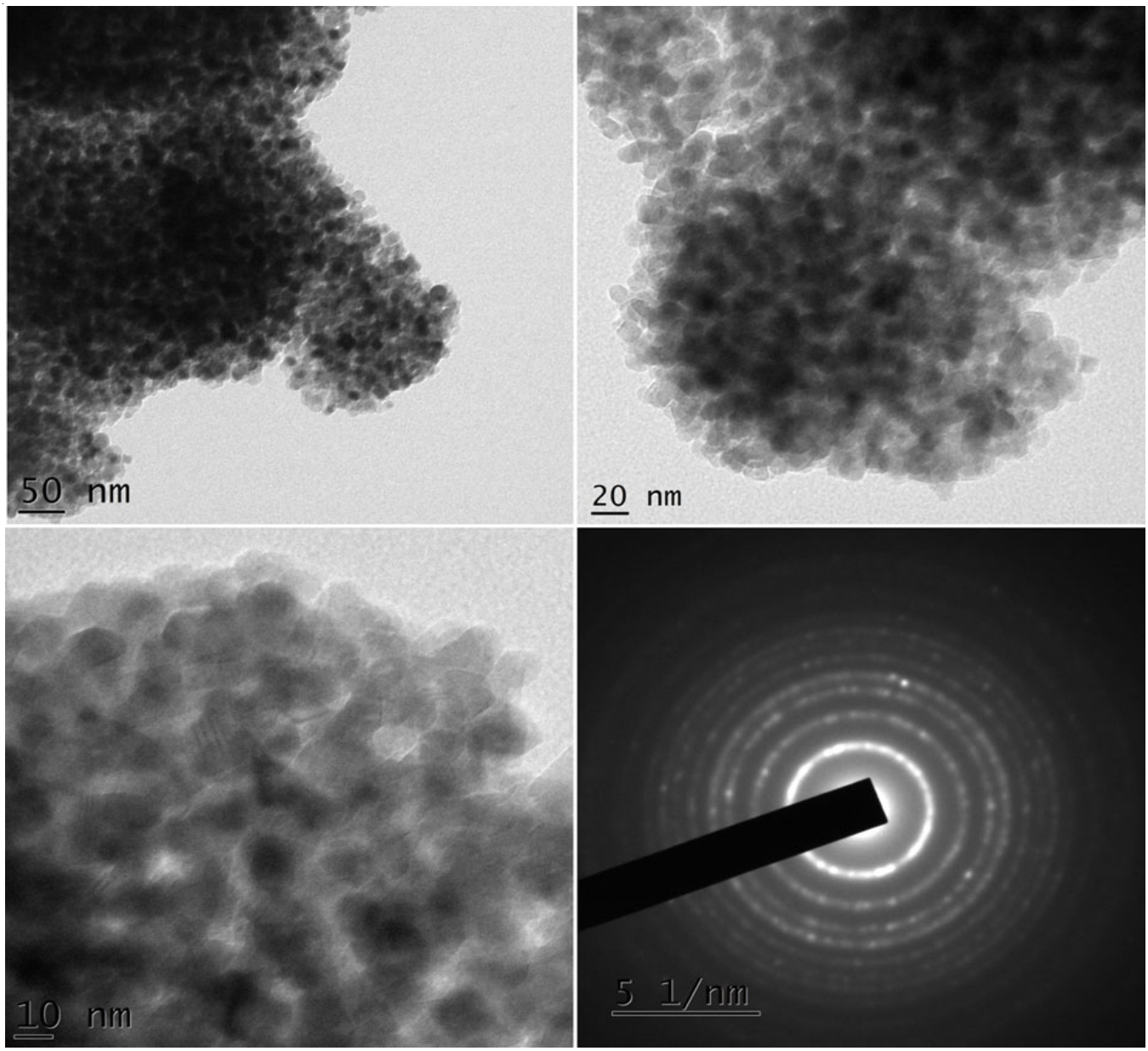

Fig. 6. TEM images of Co-ZnO nanoparticles at different magnifications

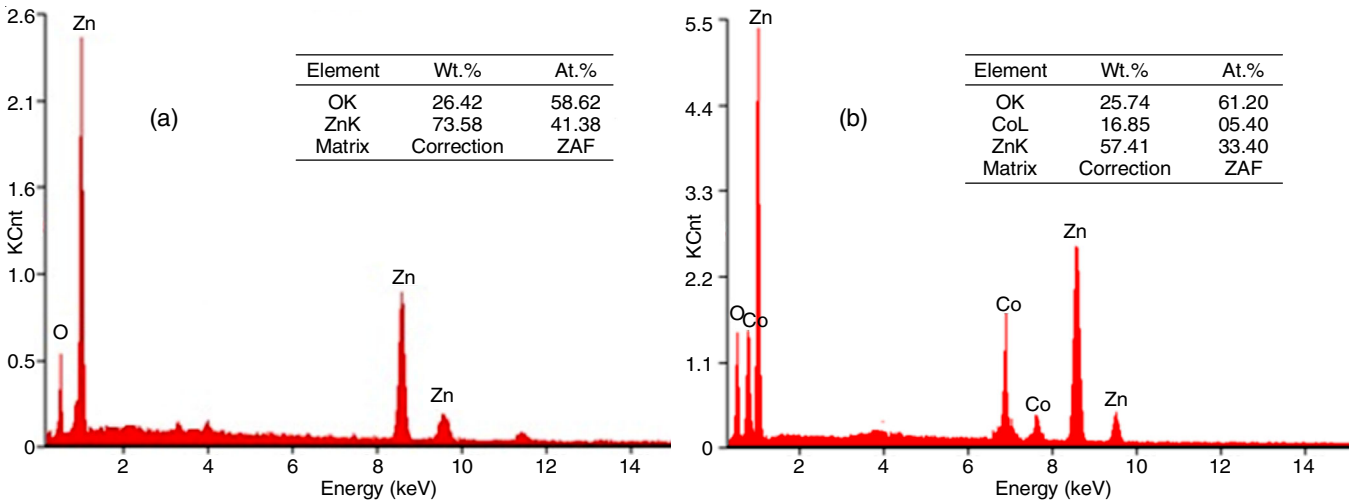

Fig. 7. Energy-dispersive X-ray spectroscopy (EDAX) analysis of (a) pure ZnO and (b) Co-ZnO nanoparticles

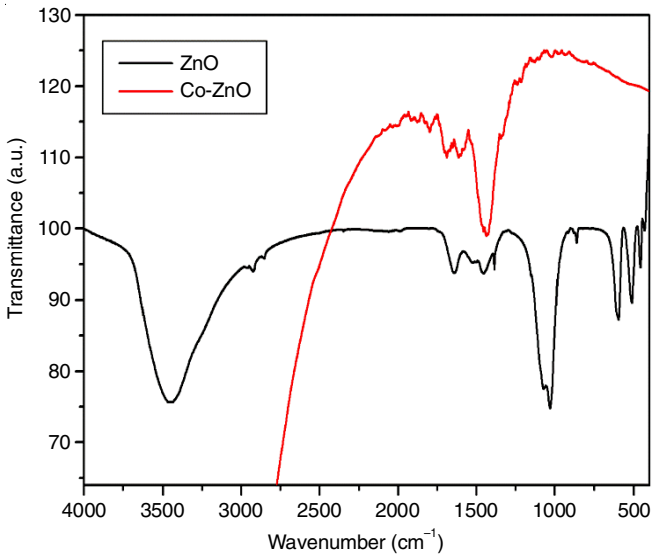

Fig. 8. Fourier transform infrared (FTIR) spectra of ZnO and Co-ZnO

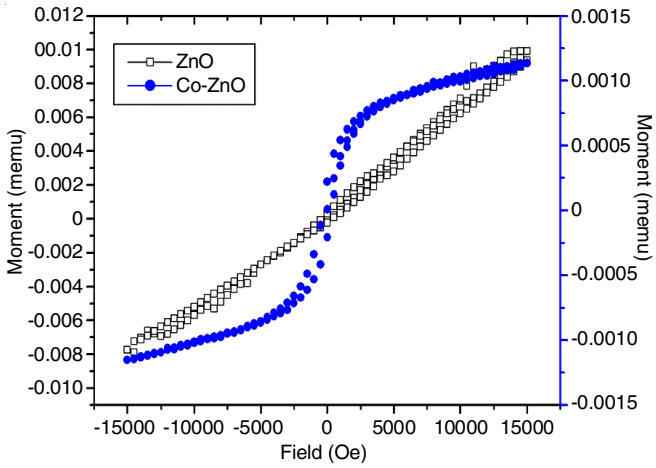

Fig. 9. Hysteresis loops of ZnO and Co-ZnO

derable increase in magnetic dipole moment. The anisotropy constant (K) of 3757.92 erg g^{-1} is remarkable higher than ZnO nanoparticles indicating a larger energy barrier for magnetization reversal [54]. In summary, the VSM data reveals that the doping of Co into ZnO nanoparticles significantly enhances its magnetic properties, particularly in terms of magnetization and magnetic moment. Nevertheless, the retentivity and coercivity values indicate that there is potential for enhancing magnetic stability and resistance to demagnetization [55].

Conclusion

The co-precipitation synthesis of pure and cobalt doped ZnO nanoparticles results in the reduced peak intensities in XRD patterns, indicating smaller crystallite sizes and increased lattice strain. The average particle size of Co doped ZnO nanoparticles is reduced to 3.82 nm and the specific surface area increases significantly, enhancing the reactivity and potential applications. Morphological studies reveal hexagonal-shaped nanoparticles with increased aggregation in Co-ZnO and EDX and FTIR analyses confirmed the successful doping of cobalt and structural modifications. The introduction of cobalt leads to a blue shift in the absorption edge, with Co-ZnO nanoparticles exhibiting an energy band gap of 3.36 eV compared to 3.25 eV for pure ZnO nanoparticles indicating improved UV absorption capabilities beneficial for the UV-related applications. The Co-ZnO nanoparticles also show enhanced photocatalytic activity and emit stronger violet-blue and blue-green light in PL spectra, attributed to the presence of Co^{2+} ions and defects, suggesting potential in photocatalysis and light-emitting applications. Moreover, cobalt incorporation significantly enhances the magnetic properties of ZnO, with Co-ZnO nanoparticles exhibiting a high magnetization of 11.448×10^{-3} emu and a magnetic moment of 0.5198 Tesla, in contrast to weak magnetic behaviour of pure ZnO making Co-ZnO suitable for spintronic and magnetic applications. Overall, the study demonstrates that cobalt doping substantially improves the properties of ZnO nanoparticles and enhancing their suitability for a range of technological applications including photocatalysis, gas sensing and spintronics.

ACKNOWLEDGEMENTS

The authors are indebted to St. Joseph's College of Arts and Science (Autonomous) for granting access to their research laboratory and library facilities, which were instrumental in the successful completion of this research work.

CONFLICT OF INTEREST

The authors declare that there is no conflict of interests regarding the publication of this article.

REFERENCES

1. G.P. Barreto, G. Morales and M.L. López Quintanilla, *J. Mater.*, **2013**, 478681 (2013); https://doi.org/10.1155/2013/478681
2. R. Yang, X. Qu and M.H. Wang, *Micro & Nano Lett.*, **13**, 1506 (2018); https://doi.org/10.1049/mnl.2018.0150
3. P.S. Sundaram, T. Sangeetha, S. Rajakarthihan, R. Vijayalaksmi, A. Elangovan and G. Arivazhagan, *Physica B*, **595**, 412342 (2020); https://doi.org/10.1016/j.physb.2020.412342
4. M. Sarfraz, N. Ahmed, K. Ul-Haq, S. Shahida and M.A. Khan, *Mater. Sci. Poland*, **37**, 280 (2019); https://doi.org/10.2478/msp-2019-0029
5. V.V. Petrov, V.V. Sysoev, I.O. Ignatieva, I.A. Gulyaeva, M.G. Volkova, A.P. Ivanishcheva, S.A. Khubezhov, Y.N. Varzarev and E.M. Bayan, *Sensors*, **23**, 5617 (2023); https://doi.org/10.3390/s23125617
6. K. Kumar, M. Chitkara, I.S. Sandhu, D. Mehta and S. Kumar, *J. Alloys Compd.*, **588**, 681 (2014); https://doi.org/10.1016/j.jallcom.2013.11.127
7. S. Senthilkumaar, K. Rajendran, S. Banerjee, T.K. Chini and V. Sengodan, *Mater. Sci. Semicond. Process.*, **11**, 6 (2008); https://doi.org/10.1016/j.mssp.2008.04.005
8. R. Poongodi, S. Senguttuvan, S. Sebastian and R. Sagayaraj, *J. Aust. Ceram. Soc.*, (2024); https://doi.org/10.1007/s41779-024-01057-z
9. S.B. Rana, R.P.P. Singh and S. Arya, *J. Mater. Sci. Mater. Electron.*, **28**, 2660 (2017); https://doi.org/10.1007/s10854-016-5843-0
10. M.K. Lima, D.M. Fernandes, M.F. Silva, M.L. Baesso, A.M. Neto, G.R. de Morais, C.V. Nakamura, A. de Oliveira Caleare, A.A.W. Hechenleitner and E.A.G. Pineda, *J. Sol-Gel Sci. Technol.*, **72**, 301 (2014); https://doi.org/10.1007/s10971-014-3310-z
11. C.M. Vladu, O.-C. Mocioiu and E.M. Soare, *Gels*, **9**, 424 (2023); https://doi.org/10.3390/gels9050424

12. R. Karthik and S. Thambidurai, *J. Alloys Compd.*, **715**, 254 (2017); https://doi.org/10.1016/j.jallcom.2017.04.298
13. N.M. Basith, J.J. Vijaya, L.J. Kennedy, M. Bououdina, S. Jenefar and V. Kaviyarasan, *J. Mater. Sci. Technol.*, **30**, 1108 (2014); https://doi.org/10.1016/j.jmst.2014.07.013
14. C. Lei, N. Sun, H. Wu, Y. Zhao, C. Yu, B.J. Janani and A. Fakhri, *Chemosphere*, **308**, 136375 (2022); https://doi.org/10.1016/j.chemosphere.2022.136375
15. O.A. Zelekew, S.G. Aragaw, F.K. Sabir, D.M. Andoshe, A.D. Duma, D.-H. Kuo, X. Chen, T.D. Desissa, B.B. Tesfamariam, G.B. Feyisa, H. Abdullah, E.T. Bekele and F.G. Aga, *Mater. Res. Express*, **8**, 025010 (2021); https://doi.org/10.1088/2053-1591/abe2d6
16. A. Chanda, S. Gupta, M. Vasundhara, S.R. Joshi, G.R. Muttae and J. Singh, *RSC Adv.*, **7**, 50527 (2017); https://doi.org/10.1039/C7RA08458G
17. A.I. Meky, M.A. Hassaan, H.A. Fetouh, A.M. Ismail and A. El Nemr, *Sci. Rep.*, **13**, 19329 (2023); https://doi.org/10.1038/s41598-023-46464-7
18. Z. Liu, M.A. Hadi, D.S. Aljuboory, F.A. Ali, M.A. Jawad, A. Al-Alwany, S.K. Hadrawi, T. Mundher, Y. Riadi, R.F. Amer and A. Fakhri, *J. Photochem. Photobiol. B Biol.*, **236**, 112571 (2022); https://doi.org/10.1016/j.jphotobiol.2022.112571
19. K.L. Foo, U. Hashim, K. Muhammad and C.H. Voon, *Nanoscale Res. Lett.*, **9**, 429 (2014); https://doi.org/10.1186/1556-276X-9-429
20. A. Muhammad, M. Sajid, M.N. Khan, M. Sheraz, A. Khalid, P. Ahmad, S. Alotibi, H.M. Al-Saidi, N. Sobahi, M.M. Alam, S. Althahban, A.M. Saeedi and H.B. Albargi, *PLoS One*, **18**, e0287322 (2023); https://doi.org/10.1371/journal.pone.0287322
21. C.S. Jincy and P. Meena, *Inorg. Chem. Commun.*, **120**, 108145 (2020); https://doi.org/10.1016/j.inoche.2020.108145
22. J. Hu, F. Gao, Z. Zhao, S. Sang, P. Li, W. Zhang, X. Zhou and Y. Chen, *Appl. Surf. Sci.*, **363**, 181 (2016); https://doi.org/10.1016/j.apsusc.2015.12.024
23. R. Bairy, *RSC Adv.*, **9**, 22302 (2019); https://doi.org/10.1039/C9RA03006A
24. B. Cullity, Elements of X-Ray Diffraction, Addison-Wesley Publ. Co. Inc., CA, USA, edn 2, p. 356 (1978).
25. J.T. Adeleke, T. Theivasanthi, M. Thiruppathi, M. Swaminathan, T. Akomolafe and A.B. Alabi, *Appl. Surf. Sci.*, **455**, 195 (2018); https://doi.org/10.1016/j.apsusc.2018.05.184
26. S. Ghosh, A. Ghosh, S. Pramanik, P.K. Kuiri, R. Sen and S.K. Neogi, *J. Phys. Conf. Ser.*, **2349**, 012014 (2022); https://doi.org/10.1088/1742-6596/2349/1/012014
27. V.K. Sharma, M. Najim, A.K. Srivastava and G.D. Varma, *J. Magn. Magn. Mater.*, **324**, 683 (2012); https://doi.org/10.1016/j.jmmm.2011.08.061
28. M. du Plessis, *Phys. Status Solidi*, **204**, 2319 (2007); https://doi.org/10.1002/pssa.200622237
29. R. Hepzi Pramila Devamani, M. Archana, K. Maheshwari and D. Susmitha, *Int. J. Eng. Sci. Invent.*, **7**, 58 (2018).
30. H.A. Varudkar, L.H. Kathwate, M.B. Awale, S.D. Lokhande, G. Umadevi, J.S. Dargad and V.D. Mote, *J. Aust. Ceram. Soc.*, **58**, 793 (2022); https://doi.org/10.1007/s41779-022-00726-1
31. T. Veeramani, C. Venkataraju, V. Porkalai and R. Sagayaraj, *Asian J. Chem.*, **35**, 2069 (2023); https://doi.org/10.14233/ajchem.2023.28041
32. J. Roberts, An Introduction to Semiconductors and Quantum Confinement, In: Using Imperfect Semiconductor Systems for Unique Identification, Springer, Cham (2017); https://doi.org/10.1007/978-3-319-67891-7_2
33. Y. Azizian-Kalandaragh, A. Khodayari, Z. Zeng, C.S. Garoufalis, S. Baskoutas and L.C. Gontard, *J. Nanopart. Res.*, **15**, 1388 (2013); https://doi.org/10.1007/s11051-012-1388-1
34. Y. Feng, Y. Zhou, Y. Liu, G. Zhang and X. Zhang, *J. Lumin.*, **119-120**, 233 (2006); https://doi.org/10.1016/j.jlumin.2005.12.040
35. M. Abdolkarimi-Mahabadi, A. Bayat and A. Mohammadi, *Theor. Exp. Chem.*, **57**, 191 (2021); https://doi.org/10.1007/s11237-021-09687-1
36. A. Ghosh and R.N.P. Choudhary, *J. Exp. Nanosci.*, **5**, 134 (2010); https://doi.org/10.1080/17458080903321829
37. H.S. Alanazi, N. Ahmad and F.A. Alharthi, *RSC Adv.*, **11**, 10194 (2021); https://doi.org/10.1039/D0RA10698D
38. M. Adeel, M. Saeed, I. Khan, M. Muneer and N. Akram, *ACS Omega*, **6**, 1426 (2021); https://doi.org/10.1021/acsomega.0c05092
39. Z. Liu, C. Wang, J. Hou, P. Wang, L. Miao, B. Lv, Y. Yang, G. You, Y. Xu, M. Zhang and H. Ci, *Environ. Sci. Pollut. Res. Int.*, **25**, 31240 (2018); https://doi.org/10.1007/s11356-018-3123-7
40. T.V.H. Luu, H.Y.X. Nguyen, Q.T. Nguyen, Q.B. Nguyen, T.H.C. Nguyen, N.C. Pham, X.D. Nguyen, T.K. Nguyen and N.N. Dao, *RSC Adv.*, **14**, 12954 (2024); https://doi.org/10.1039/D4RA00579A
41. K.S. Babu, A.R. Reddy, C. Sujatha, K.V. Reddy and A.N. Mallika, *J. Adv. Ceram.*, **2**, 260 (2013); https://doi.org/10.1007/s40145-013-0069-6
42. D. Mora-Fonz, J. Buckeridge, A.J. Logsdail, D.O. Scanlon, A.A. Sokol, S. Woodley and C.R.A. Catlow, *J. Phys. Chem. C*, **119**, 11598 (2015); https://doi.org/10.1021/acs.jpcc.5b01331
43. R.T. So, N.E. Blair and A.L. Masterson, *Environ. Chem. Lett.*, **18**, 1725 (2020); https://doi.org/10.1007/s10311-020-01027-4
44. A. Saini, S. Kumar, H. Kaur, J. Gaur, G. Singh, M. Kaur, S. Kumar, R. Limbu, Supreet, R. Pal and N. Kaur, *Interaction*, **245**, 174 (2024); https://doi.org/10.1007/s10751-024-02012-x
45. X. Guo, L. Liu, J. Wu, J. Fan and Y. Wu, *RSC Adv.*, **8**, 4214 (2018); https://doi.org/10.1039/C7RA09894D
46. C.C. Yu, K.Y. Chiang, M. Okuno, T. Seki, T. Ohto, X. Yu, V. Korepanov, H. Hamaguchi, M. Bonn, J. Hunger and Y. Nagata, *Nat. Commun.*, **11**, 5977 (2020); https://doi.org/10.1038/s41467-020-19759-w
47. S. Kammoun and J.E. ghoul, *J. Mater. Sci. Mater. Electron.*, **32**, 7215 (2021); https://doi.org/10.1007/s10854-021-05430-7
48. A. Modwi, K.K. Taha, L. Khezami, A.S. Al-Ayed, O.K. Al-Duaij, M. Khairy and M. Bououdina, *J. Inorg. Organomet. Polym. Mater.*, **30**, 2633 (2020); https://doi.org/10.1007/s10904-019-01425-4
49. L. Chellappan, B. Thangaraj, N. Muthukurumban and V. Gurusamy, *J. Fluoresc.*, (2024); https://doi.org/10.1007/s10895-024-03605-z
50. A.F. AL Naim, A. Solieman and E.R. Shaaban, *J. Mater. Sci. Mater. Electron.*, **31**, 3613 (2020); https://doi.org/10.1007/s10854-020-02916-8
51. K. Safeen, A. Safeen, D. Arif, W.H. Shah, A. Ali, G. Ali, F. Hussain, N. Imran, A. Ullah Shah, A. Alataway, A.Z. Dewidar, H.O. Elansary, M. Al-Yafrsi and K.S. Ahmad, *Water*, **15**, 1470 (2023); https://doi.org/10.3390/w15081470
52. P.Y. Zhang, R. Hiergeist, J. Lüdke, M. Albrecht and H.L. Ge, *J. Appl. Phys.*, **108**, 043905 (2010); https://doi.org/10.1063/1.3457105
53. R. Sagayaraj, S. Aravazhi and G. Chandrasekaran, *Int. Nano Lett.*, **11**, 307 (2021); https://doi.org/10.1007/s40089-021-00343-z
54. T.C. Ji, M.X. Pan, H.L. Ge, Q. Wu and P.-Y. Zhang, *Rare Metals*, **40**, 1232 (2021); https://doi.org/10.1007/s12598-020-01405-5
55. L.B. Arruda, D.M.G. Leite, M.O. Orlandi, W.A. Ortiz and P.N. Lisboa-Filho, *J. Supercond. Nov. Magn.*, **26**, 2515 (2013); https://doi.org/10.1007/s10948-012-1417-4